Zlotnik, S., Díez, P., Hierarchical X-FEM for n-phase flow (n>2), *Computer Methods in Applied Mechanics and Engineering*, Vol. 198 Issues 30-32, pp. 2329-2338, 2009

Hierarchical X–FEM for n–phase flow $(n > 2)$

Sergio Zlotnik [a] Pedro Díez [b,*]

[a] *Group of Dynamics of the Lithosphere (GDL) Institute of Earth Sciences "Jaume Almera", CSIC Lluís Solé i Sabarís s/n, 08028 Barcelona, Spain*

[b] *Laboratori de Càlcul Numèric, Departament de Matemàtica Aplicada III Universitat Politècnica de Catalunya Campus Nord UPC, 08034 Barcelona, Spain*

Abstract

The eXtended Finite Element Method (X–FEM) has been successfully used in two-phase flow problems involving a moving interface. In order to simulate problems involving more than two phases, the X–FEM has to be further eXtended. The proposed approach is presented in the case of a quasistatic Stokes n-phase flow and it is based on using an ordered collection of level set functions to describe the location of the phases. A level set hierarchy allows describing triple junctions avoiding overlapping or "voids" between materials. Moreover, an enriched solution accounting for several simultaneous phases inside one element is proposed. The interpolation functions corresponding to the enriched degrees of freedom require redefining the associated ridge function accounting for all the level sets.

The computational implementation of this scheme involves calculating integrals in elements having several materials inside. An adaptive quadrature accounting for the interfaces locations is proposed to accurately compute these integrals.

Examples of the hierarchical X–FEM approach are given for a n–phase Stokes problem in 2 and 3 dimensions.

Key words: multiphase flow; level set methods; enrichment; eXtended Finite Element Method (X–FEM)

* Corresponding author.
Email addresses: szlotnik@ija.csic.es (Sergio Zlotnik), pedro.diez@upc.es (Pedro Díez).
URLs: www.ija.csic.es/gt/sergioz/ (Sergio Zlotnik), www-lacan.upc.es (Pedro Díez).

1 Introduction

Level set methods are becoming increasingly popular for the solution of fluid problems involving moving interfaces [10]. In the two-phase case, the level set methods can predict the evolution of complex interfaces including changes in topology such as deforming bubbles, break up and coalescence, etc. This kind of flow is encountered in a wide range of industrial and natural applications. Since the introduction of the level set method by Osher and Sethian [8], a large amount of bibliography has been published. See, for instance, the cited review by Sethian and Smereka [10] and the work by Osher and Fedkiw [7].

Despite the term *multiphase* is widely used in the literature, most works using level sets for tracking material interfaces limit the number of phases to two. This restriction comes from the use of the sign of a level set function to describe the materials location. There are some works handling n–phase models ($n > 2$) based on several level set functions. For example, Tan and Zabaras [11] use the level set technique combined with features of front tracking methods to model the microstructure evolution in the solidification of multi–component alloys. In this work each component is defined by a level set function: the sign limits the solid–liquid interface. Two algorithms to simulate triple junctions where the interfaces motion depends on surface tension and bulk energies were proposed by Zhao et. al. [13] and Ruuth [9]. These works use a number of level set functions equal to the number of materials. They require adding some further restrictions to the model in order to prevent overlapping or vacuum between phases. Recently Dolbow et al. [**?**] presented a similar technique to enforce conservation laws across interfaces described using the Patterned Interface Reconstruction method.

In this work we propose a different approach to describe and to model n-phase flow problems based on X–FEM. The main ingredients are: level sets and an enriched solution. We avoid the geometrical inconsistency (overlapping or voids) by introducing a hierarchy between the level sets. Moreover, the enrichment of the solution is extended to account for triple (or multiple) junctions inside an element. This allows for handling gradient discontinuities across the interface. In the following sections the hierarchy between level sets and the multiple enrichment are presented in the context of a n-phase flow problem. Computational considerations on how to integrate discontinuous function on elements are discussed next. Finally, in order to show the behavior of the proposed approach we present several application examples in 2D and 3D of n–phase flow problems driven by gravitational forces.

2 Problem statement

The hierarchical X–FEM is developed to simulate a flow problem with n phases ($n > 2$). An n–phase fluid governed by the Stokes equation is considered. The inertia term is neglected and the problem is thus quasi–static. This is a common situation in geophysical modeling, where creeping (very slow) flow arises (e.g. [14]). The governing equations are written in terms of velocity $\mathbf{u}$ and pressure p as

$$\nabla \cdot (\eta \nabla^{\mathrm{s}} \mathbf{u}) + \nabla p = \rho \mathbf{g}, \tag{1a}$$

$$\nabla \cdot \mathbf{u} = 0 \tag{1b}$$

where η is the viscosity, ρ the density, and $\mathbf{g}$ the gravitational acceleration vector. The symmetrized gradient operator ∇^{s} is defined as $\frac{1}{2}(\nabla^{\top} + \nabla)$. Density and viscosity fields are constant in each phase and discontinuous across interfaces. Equation (1) is quasi–static and it does not contain any explicit time dependence; the transient character of the solution is due to the motion of the phases. For the sake of a simple presentation, the problem is described by equation (1), that is the expression of the balance law in strong form. The complete description of the Boundary Value Problem is therefore omitted and would require, along with the boundary conditions, to explicitly enforce the continuity of the normal stresses across the interfaces where the viscosity is discontinuous. This is naturally treated in the weak form of the problem adopted in the practical implementation. The Stokes problem is discretized using the standard mini element (triangular element with enhanced linear velocities and linear pressure), which is the simpler option fulfilling the LBB condition.

The location of the different phases is described by a collection of level set functions. The level sets represent material properties and they are consequently transported by the motion of the fluid. Thus the evolution of each one of the level sets, describing phase locations, is determined by pure advection equation

$$\dot{\phi}^{(i)} + \mathbf{u} \cdot \nabla \phi^{(i)} = 0 \tag{2}$$

where $\mathbf{u}$ is the velocity field, solution of the Stokes problem (1), and $\phi^{(i)}$ is the level set number i. In the applications, equation (2) is solved using linear triangular elements and using the two-step third order Taylor-Galerkin time-marching scheme, especially designed to deal with the advective character of the problem [3].

3 Describing a n–phase fluid with $n-1$ level sets

The level set technique is widely used in two and three dimensions to track one free interface between two materials, see for example [12,1,14]. This section is devoted to generalize this strategy to n-phase flows.

3.1 Two phases with a single level set

The location of the interface between two materials is described using a level set function $\phi^{(1)}$. The superscript $^{(1)}$ denotes the number of level set and it is useful when 3 or more phases have to be described. This superscript is not strictly necessary in this section, it is used here to keep a consistent notation in the following sections. The sign of the level set $\phi^{(1)}$ describes a partition of the domain Ω in two subdomains Ω_1 and Ω_2 using the following sign convention

$$\phi^{(1)}(\mathbf{x},t) = \begin{cases} > 0 & \text{for } \mathbf{x} \in \Omega_1 \\ = 0 & \text{for } \mathbf{x} \text{ on the interface} \\ < 0 & \text{for } \mathbf{x} \in \Omega_2 \end{cases} \tag{3}$$

where $\mathbf{x}$ stands for a point in Ω and t is the time. The interface is the set of points where the level set field vanishes. An example of partition is shown in Figure 1. Initially the level set $\phi^{(1)}$ is defined as a signed distance to the interface. Far enough from the interface, $\phi^{(1)}$ is truncated by positive and negative cutoff values. The resulting level set function describes the position of the interface independently of the computational mesh, thus the same mesh can be used trough the entire simulation avoiding remeshing procedures.

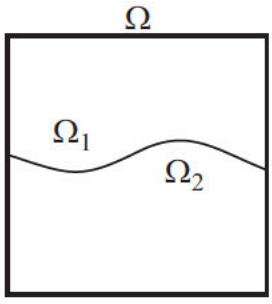

Fig. 1. One level set function splits the domain in two subdomains corresponding to the different phases.

3.2 *Tracking more than two phases: hierarchy of level sets*

One level set allows for describing only two phases (two subdomains). To include a third subdomain Ω_3 a second level set function $\phi^{(2)}$ is needed. We propose to assign a *hierarchy* to the level set functions: the subdomain Ω_1 is determined by the first level set $\phi^{(1)}$ as

$$\phi^{(1)}(\mathbf{x},t) = \begin{cases} > 0 & \text{for } \mathbf{x} \in \Omega_1 \\ \leq 0 & \text{for } \mathbf{x} \notin \Omega_1 \end{cases} \tag{4}$$

The curve where the level set $\phi^{(1)}(\mathbf{x},t)$ equals zero is the interface between the first phase and the rest of the domain. That is, either the second or the third phase. The remaining part in the simulation domain ($\mathbf{x} \in \Omega \backslash \Omega_1$) is split by the second level set $\phi^{(2)}$ as

$$\text{for } \mathbf{x} \notin \Omega_1,\ \phi^{(2)}(\mathbf{x},t) = \begin{cases} > 0 & \text{for } \mathbf{x} \in \Omega_2 \\ \leq 0 & \text{for } \mathbf{x} \in \Omega_3 \end{cases} \tag{5}$$

determining the location of the second and third sub domains. Note that the second level set does not have any influence where the first level set is positive. We say that the first level set is "prior to" —or has upper hierarchy than— the second level set. Figure 2 shows the partition of the domain by two hierarchical level sets into three subdomains.

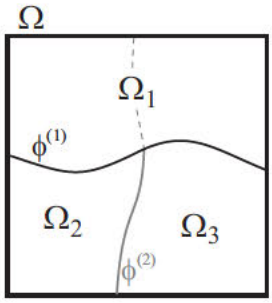

Fig. 2. Two hierarchical level sets describe three material sub domains. The second level set $\phi^{(2)}$ is relevant only where the first level set $\phi^{(1)}$ is negative. Dashed line represents the level set with lower hierarchy eclipsed by the first level set.

The hierarchy can be extended to the general case of n phases being tracked by $n-1$ level sets. The level set number i, $\phi^{(i)}$, defines the location of the phase i as follows

$$\text{for } \mathbf{x} \notin \bigcup_{j=1}^{i-1} \Omega_j,\ \phi^{(i)}(\mathbf{x},t) = \begin{cases} > 0 & \text{for } \mathbf{x} \in \Omega_i \\ \leq 0 & \text{for } \mathbf{x} \notin \Omega_i \end{cases} \tag{6}$$

for all $i = 1, \ldots, n-2$. The level set with lowest hierarchy, $\phi^{(n-1)}$, determines the location of the last two phases in the remaining space as

$$\text{for } \mathbf{x} \notin \bigcup_{j=1}^{n-2} \Omega_j, \;\; \phi^{(n-1)}(\mathbf{x}, t) = \begin{cases} > 0 & \text{for } \mathbf{x} \in \Omega_{n-1} \\ \leq 0 & \text{for } \mathbf{x} \in \Omega_n \end{cases} \tag{7}$$

In this approach the positive part of the i–th level set defines the material subdomain Ω_i and the negative region have to be partitioned by the level sets with less hierarchy. Figure 3 illustrates a partition into four subdomains by three level sets.

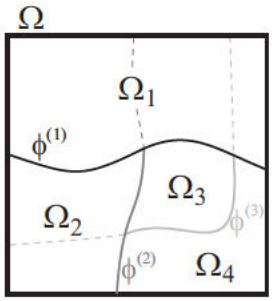

Fig. 3. Three hierarchical level sets allow describing four material phases. The last level set $\phi^{(3)}$ acts only where the first two level sets are negative.

Note that the interface described by a level set does not need to be simply connected, thus, assigning the right hierarchy to the level sets any material configuration can be stated. See a more complex configuration in Figure 4.

The hierarchical representation may describe any topology and distribution of the phases. The question arises if the same hierarchy may be used all along the evolution process. According to our experience, if the hierarchy is selected properly at the initial stage, all the topology changes during the evolution can be handled with a unique hierarchy. Selecting this initial description could require knowing a priori the main topological trends of the solution (i.e. which are the phases that may be detached or split).

A compact expression for the domains defined by the hierarchical level sets uses the McCauley brackets defined by

$$\langle \phi \rangle = 1/2 \; (\phi + |\phi|) \, .$$

Thus, the domain Ω_i reads

$$\Omega_i = \text{supp} \left\{ \langle \phi^i \rangle \prod_{j=1}^{i-1} \langle -\phi^j \rangle \right\} .$$

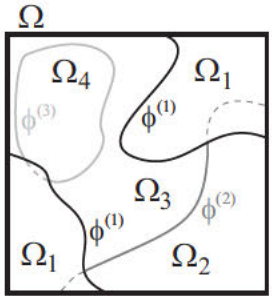

Fig. 4. A complex material distribution can be described with the hierarchical approach. Here, $\phi^{(1)}$ describes a disconnected interface.

It is worth remarking that in all the presented examples there is no need of re-initializing the level sets along the time integration. Note, however, that in case it is needed, re-initializing in this hierarchical context is simple because every level set can be treated separately.

4 X–FEM enrichment

The interface described by a level set does not need to conform with mesh edges. That leads to multiphase elements with different materials inside. Across the interface a gradient discontinuity arises and therefore the X–FEM enriches the numerical solution in order to include gradient jumps.

The interpolation of velocity $\mathbf{u}$ on the enriched elements is composed by the standard finite element part plus an enriched part. The latter involves additional degrees of freedom $\mathbf{a}_j$ and its associated interpolation functions M_j

$$\mathbf{u}_h(\mathbf{x},t) = \sum_{j\in\mathcal{N}} \mathbf{u}_j(t)\, N_j(\mathbf{x}) + \sum_{j\in\mathcal{N}_{enr}} \mathbf{a}_j(t)\, M_j(\mathbf{x}) \tag{8}$$

where $\mathcal{N}$ is the set of standard finite element velocity degrees of freedom and $\mathcal{N}_{enr}$ is the set of enriched degrees of freedom. The $\mathcal{N}_{enr}$ set evolves through time affecting the nodes located along the interface and needs to be recomputed at each time step after level set movement. The pressure field p is enriched in a similar way.

The interpolation function M_j, associated with enriched degrees of freedom, is constructed as the product of standard nodal shape functions and a ridge function denoted by R,

$$M_j = N_j R. \tag{9}$$

The R function is based on the level set and has a "crest" over the interface between materials. Different ridge functions have been proposed in the litera-

ture, see for example [1,6]. In the following a ridge function properly defined in the elements with multiple interfaces in introduced. The rationale follows the ideas proposed by Moës and co-authors in [6].

4.1 Two phases, one Ridge

In a two–phase simulation the single interface is described by a unique level set. The enriched elements are those which are crossed by the interface (where $\phi^{(1)}$ vanishes) and the ridge function can be constructed as [6]

$$R = \sum_{j \in \mathcal{N}_{enr}} \left|\phi_j^{(1)}\right| N_j - \left| \sum_{j \in \mathcal{N}_{enr}} \phi_j^{(1)} N_j \right|. \tag{10}$$

Note that this function vanishes in the element edges not crossed by the level set. Thus, the interpolation functions of enriched elements conform with those of not-enriched elements. This kind of function is depicted in Figure 5.

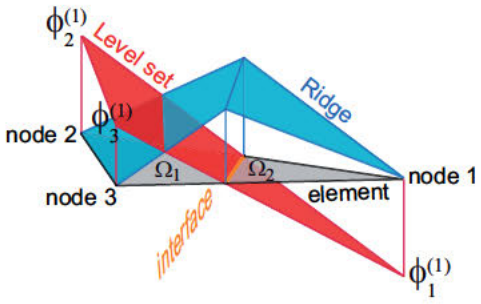

Fig. 5. Ridge function R based on one level set $\phi^{(1)}$.

4.2 Ridge function for two level sets

The 3–phase configuration requires reviewing the basic operations in the previously described approach for the 2–phase flow. Firstly, the detection of enriched element has to include the level set hierarchy. Secondly, the triple junction case, where two level sets intersects one element has to be considered and properly resolved. Note that the degrees of freedom $\mathbf{a}_j$, for $j \in \mathcal{N}_{enr}$, as introduced in equation (8) to enrich the FE approximation, are associated with the nodes, not with the elements. Nevertheless, all the nodes to be enriched belong to elements crossed by some interface and, in practice, determining the *enriched* elements is sufficient to locate the enriched nodes. Moreover, in contrast with other enrichment techniques [1], in this case the support of the enrichment functions M_i is restricted to the so-called enriched elements.

The detection for elements to be enriched is the following: elements have to be marked to enrich if they are crossed by the interface described by $\phi^{(1)}$ or crossed by the interface described by $\phi^{(2)}$ and being $\phi^{(1)}$ negative. This statement is easily encoded. In the code repository
(or in `http://www.ija.csic.es/gt/sergioz/main/codes.htm`) we provide a highly vectorized MATLAB function named `crossedByLevelSet` accepting any element type in any number of dimensions and returns if the element has to be enriched or not.

The ridge function in elements crossed by only the k–th level set is defined as in the previous case and denoted by $r^{(k)}$:

$$r^{(k)} = \sum_{j \in \mathcal{N}_{enr}} \left|\phi_j^{(k)}\right| N_j - \left| \sum_{j \in \mathcal{N}_{enr}} \phi_j^{(k)} N_j \right| \tag{11}$$

where k is 1 or 2 for elements crossed by $\phi^{(1)}$ or $\phi^{(2)}$, respectively. In the elements containing only one interface the ridge function is equal to the corresponding single rigde, that is $R = r^{(k)}$.

In the triple junction case, where two interfaces meet in one element, the ridge function must account for both level sets and the hierarchy between them. In this case R is defined as

$$R = r^{(1)} + r^{(2)} C^{(1)} \tag{12}$$

where the cutoff function $C^{(1)}$ introduces the level set hierarchy and is defined as

$$C^{(1)}(\mathbf{x}) = \begin{cases} 1 & \text{if } \phi^{(1)} \leq 0 \\ r^{(1)}_{\text{norm}} & \text{otherwise} \end{cases} \tag{13}$$

Here, $r^{(1)}_{\text{norm}}$ is the normalized ridge of the level set $\phi^{(1)}$. The normalization process modifies the ridge leaving its crest with a constant value equal to one. Therefore, the cutoff function $C^{(1)}$ is continuous across the interface: $r^{(1)}_{\text{norm}} = 1$ at the interface. The normalized ridge function, $r^{(1)}_{\text{norm}}$, is defined as

$$r^{(1)}_{\text{norm}} = \frac{\displaystyle\sum_{j \in \mathcal{N}_{enr}} \left|\phi_j^{(1)}\right| N_j - \left| \sum_{j \in \mathcal{N}_{enr}} \phi_j^{(1)} N_j \right|}{\displaystyle\sum_{j \in \mathcal{N}_{enr}} \left|\phi_j^{(1)}\right| N_j} \tag{14}$$

The cutoff function $C^{(1)}$ restricts the full effect of the second ridge $r^{(2)}$ to the region where the first level set $\phi^{(1)}$ is negative. Moreover it smoothly kills the value of $r^{(2)}$ in the side of the first interface where $\phi^{(1)}$ is positive. Despite the definition (14) does not include the time explicitly, it inherits the time dependence of the level sets location, so $r^{(i)}$ (and consequently R) changes

through time. The illustration of the proposed ridge function for an element crossed by two level sets is shown in Figure 6.

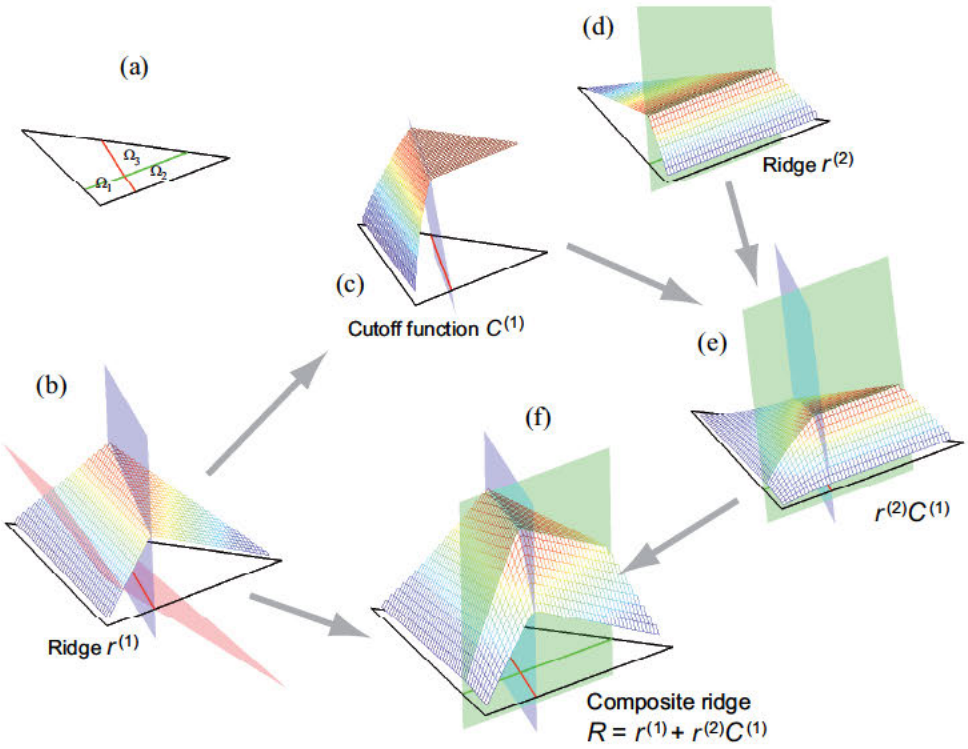

Fig. 6. Composite ridge based in two hierarchical level sets. Plot (a) shows the element and the position of the interfaces. The ridge $r^{(1)}$ of the first level set $\phi^{(1)}$ is shown in (b). The cutoff function $C^{(1)}$ based on the first level set is shown in (c). The ridge $r^{(2)}$ of the second level set is shown in (d). Plot (e) shows the product $r^{(2)}C^{(1)}$. Finally, (f) shows the complete composite ridge $R = r^{(1)} + r^{(2)}C^{(1)}$.

The elements when this multiple-enrichment has to be applied are more than the obvious: some of them cannot be detected at the first glance an accurate analysis is required to avoid forgetting them. The obvious criterion is: an element is required to be multiple enriched if it is crossed by two *active* interfaces. This is not sufficient to guarantee the overall consistency (continuity) of the interpolation. This is illustrated in the following example. The elements numbered 1 and 2 in Figure 7 require multiple–enrichment because they have three different materials in its interior. Note that due to the hierarchy of level sets, the element number 3 has only two materials inside. Nevertheless, element number 3 must be multiple–enriched to guarantee the continuity of the interpolation functions. The multiple–enrichment of element 3, is needed to guaranty the conformity with its neighbors; the left side of the element matches with element 2 because both account for both level sets. The right side of the element is not affected by the second level set, as its ridge is zero on the edge and, finally, the ridge R on the upper side of element 3 is zero because of the ridge $r^{(1)}$, corresponding to the level set $\phi^{(1)}$, which vanishes

on that side.

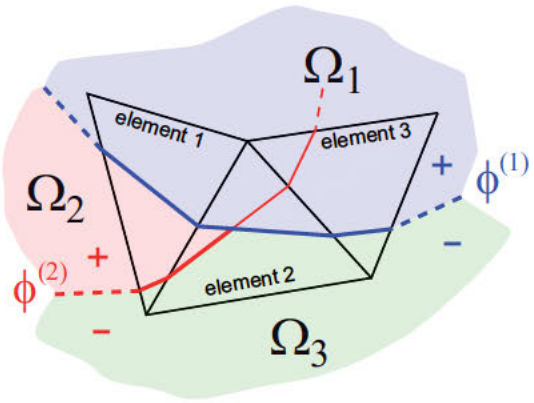

Fig. 7. Example of elements whose ridge must be based on both level sets. Note that the second level set, $\phi^{(2)}$, does not define an interface where the first level set $\phi^{(1)}$ is positive (element 3). Nevertheless, the ridge function in the element 3 must be constructed using both level sets to guarantee continuity.

4.2.1 General case

The latter example is extended to the general case where n level sets simultaneously cross one element. The general definition of the resulting ridge is

$$R = r^{(1)} + \sum_{i=2}^{n-1} r^{(i)} C^{(i-1)} \tag{15}$$

Note that the ridge function $r^{(i)}$ of a level set not crossing the element is zero, thus adding all ridges $r^{(i)}$ to obtain R only accounts for pertinent level sets. The $C^{(i)}$ cutoff function defined as

$$C^{(i)}(\mathbf{x}) = \begin{cases} 1 & \text{if } \phi^{(i)}(\mathbf{x}) \leq 0 \\ r^{(i)}_{\text{norm}} & \text{otherwise} \end{cases} \tag{16}$$

Same as for $r^{(1)}_{\text{norm}}$, the normalized ridge $r^{(i)}_{\text{norm}}$ is the ridge $r^{(i)}$ with unitary crest, that is

$$
\begin{aligned}
r^{(i)}_{\text{norm}} &= \frac{\displaystyle\sum_{j\in\mathcal{N}_{enr}} \left|\phi^{(i)}_j\right| N_j - \left|\sum_{j\in\mathcal{N}_{enr}} \phi^{(i)}_j N_j\right|}{\displaystyle\sum_{j\in\mathcal{N}_{enr}} \left|\phi^{(i)}_j\right| N_j} \\
&= 1 - \frac{\left|\displaystyle\sum_{j\in\mathcal{N}_{enr}} \phi^{(i)}_j\, N_j\right|}{\displaystyle\sum_{j\in\mathcal{N}_{enr}} \left|\phi^{(i)}_j\right| N_j}
\end{aligned}
\tag{17}
$$

4.3 Numerical integration in multiphase elements

The X–FEM implementation requires computing integrals of discontinuous functions in elements crossed by the level set. The traditional quadrature rules, for example Gauss quadratures, are designed to integrate polynomials and regular functions that are fairly approximated by polynomials. These quadratures are not expected to show a good performance integrations discontinuous functions.

To preclude the problem associated with discontinuities and to calculate the integrals accurately it is usual to split multiphase elements in single-material subdomains. In these subdomains functions are continuous and standard quadratures provide accurate results.

The computational effort and algorithmic involvement of defining each integration subdomain depends on the shape of the elements and on the number of spatial dimensions involved. For example, with only one level set triangular elements are split into one triangle and one quadrilateral or into two triangles. This geometrical splitting is coded straightforwardly based on the element geometry and the level set. The same operation for quadrilateral elements is much mode cumbersome because the number of possible geometrical divisions is much higher. In particular, the splitting of a quadrilateral generates three-, four- and five-sides polygons. Further subdivisions are needed to integrate in five-sided shapes with standard quadratures.

In three dimensions the number shapes generated by cutting elements by one level set increases rapidly. Tetrahedral elements cutted by a plane interface must by split into five single-material tetrahedrals. This partition of the element is much more complicated to code and computationally demanding. The element subdivision is increasingly involved if the number of phases is larger.

Using the hierarchical level set approach element are split in polygonal single-material subdomains with any number of sides. The general case of detecting

each one of the n-side polygons is complex to code and computationally expensive. In this situation a numerical quadrature acting in the whole element (without any geometrical subdivision)is even mode interesting.

The first trial is using a simple (low order) but very populated quadrature rule. Intuitively, it is clear that a large number of quadrature points should allow for integrating the discontinuity accurately. A uniformly refined overkill quadrature should by accurate enough, though ignoring the location of the interface where the discontinuity takes place. This integration method should be used only in elements crossed by several level sets. As they are expected to be only a few, using a costly quadrature does not practically affect the overall computation time. This strategy is used in a triangular element crossed by one level set with a trapezoidal quadrature on a uniformly refined triangular submesh. This approach is straightforward to implement as a recursive function and thus the number of quadrature points can be increased to any desired value. Moreover, due to the simplicity of the quadrature (first order) is expected to be robust and to minimize the error in the region where the function is discontinuous. The quadrature is implemented recursively based in the split of a triangular element into four similar triangles. It is tested in the computation of an elementary matrix corresponding to the discretization of the Stokes problem (1b). The element under consideration is affected by only one level set; the exact solution is in that case easily calculated by splitting the element into three triangles.

The accuracy obtained with this trapezoidal quadrature is disappointing: to obtain a relative error of 10^{-2} in all the coefficients of the elementary matrix, 8385 integration points are needed. To decrease this error to 6×10^{-3}, the number of integration points required is 33153. A large number of integration points does not reduce the order of the relative error: using 525825 integration points still produces a relative error larger than 10^{-3}. This number of integration points exceeds the values that are computationally acceptable in practice. Table 1 displays the relative errors obtained for different levels of recursion.

We conclude that the previous integration method has to be discarded and an alternative integration procedure is required. Thus, we propose using an adaptive scheme increasing the resolution along the interfaces described by the level set functions. The adaptive quadrature is designed to increase the number of points optimizing their location.

The resolution of the quadrature is improved along the interface using an adaptive recursive subdivision of the element into smaller elements. Starting from a coarse quadrature in the triangle, it is successively refined by splitting into four triangles all those crossed by the discontinuity. This is illustrated in Figure 8, showing six level of adaptive refinement. The accuracy of this iterative process is controlled by comparing two successive approximations. In

practice, the number of levels of refinement is such that the difference between the last two levels is below the prescribed tolerance.

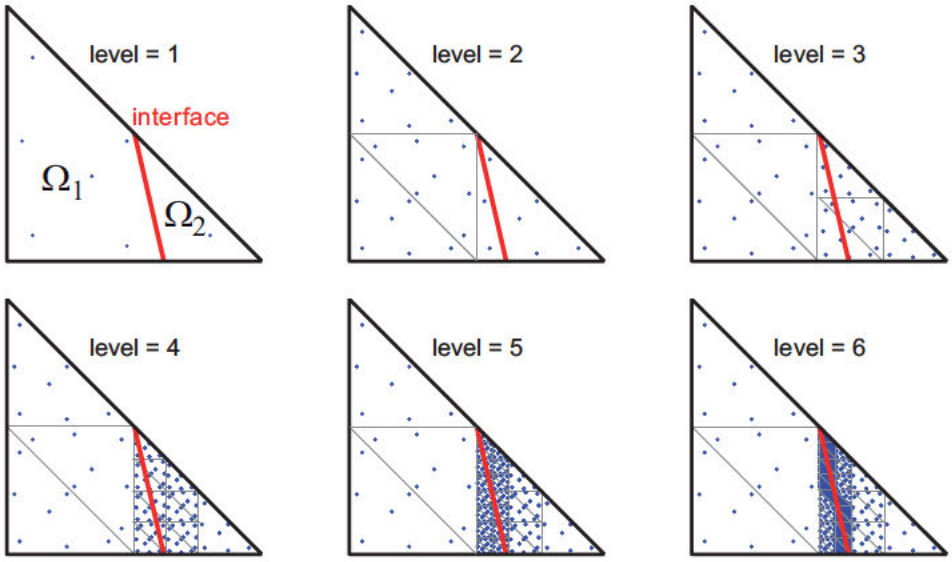

Fig. 8. Location of integration points in the adaptive quadrature. The number of integration points in the successively refined quadrature are 7, 29, 49, 112, 259 and 574. The accuracy obtained is shown in table 1.

A simple Gaussian-type quadrature is sufficient to integrate the subdivisions not affected by the discontinuity. In the particular case of the Stokes problem (1) the integrated functions are polynomials of degree four at most. Thus, a seven-point gaussian quadrature of order four is selected in every single subdivision.

Trapezoidal quadrature			Adaptive quadrature		
Recursive level	Number of points	Max rel error	Recursive level	Number of points	Max rel error
1	3	55.6	1	7	5.4
2	6	13.3	2	28	0.51
3	15	3.7	3	49	0.38
4	45	1.6	4	112	0.076
5	153	0.4	5	259	0.036
6	561	0.08	6	574	0.0047
7	2145	0.03	7	1225	0.0019
8	8385	0.01	8	2548	0.00029
9	33153	0.006	9	5215	9.65×10^{-5}
10	131841	0.0038	10	10570	1.90×10^{-5}
11	525825	0.0019	11	21301	8.71×10^{-6}

Table 1
Accuracy of the uniform trapezoid and adaptive quadratures. The relative error refers to the maximum in the coefficients of the elementary matrix for the Stokes problem. The location of the interface is same as in Figure 8.

The adaptive quadrature drastically improves the accuracy with respect to the uniform trapezoidal integration and sufficient accuracy is obtained with a reasonable amount of integration points. Recall that this strategy is only needed in the elements affected by the interface. However, the computational effort to integrate the stiffness matrices in these elements is important.

An alternative integration procedure is based on the Constrained Delaunay Triangulation (or tetrahedralization, in both cases corresponding to the acronym CDT), as used for instance by Wall and coauthors [4]. This idea is allowing to automatically split the element into monophasic subdomains and thus to use in each subdomain a simple quadrature. A second alternative is provided by Daux et al. [2] based in the recursive splitting of the domains (triangles or tetrahedra) following the interfaces. Comparing the cost of these approaches with the one introduced here is beyond the scope of this paper.

The adaptive quadrature is used in examples presented in next section providing satisfactory results.

5 Numerical examples

The strategy developed in the previous Sections is tested here in some standard application examples. The n–phase X–FEM approach is used to simulate gravitational Rayleigh–Taylor instabilities in 2 and 3 dimensions. The models are composed by $n \geq 3$ immiscible materials governed by the Stokes equation (1). The driving force in all models is the gravity; the density contrast makes the buoyant layers (with lower density than the overlying layers) to flow upward and the denser layers to flow downward.

5.1 Two-dimensional 3-phase instabilities

The initial configuration of the following examples is given by the location of three materials, as shown in Figure 9. Two level sets are regarded to describe this configuration. The first level set in hierarchy is the one corresponding to the upper denser material. The second level set describes the vertical interface between the two lighter materials. Note than the vertical interface does not continue through the upper material due to the level set hierarchy. The upper layer is ten times denser than the two lower materials. The lower materials have different viscosity, thus the resulting configuration (the formed diapir) looses its vertical axis of symmetry.

The consistency of the proposed strategy is analyzed observing the evolution of

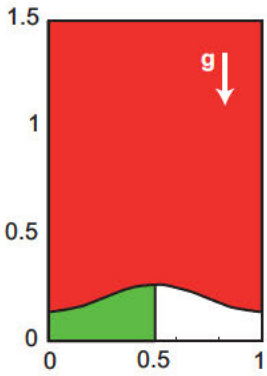

Fig. 9. Initial configuration with three materials. The upper material is denser than the other two. The viscosity of the materials is indicated in Figure 13.

different indicators. First, the vertical velocity of the instability (the velocity of the growing diapir) at a given moment in time is used to study the consistence of the solution. Note that this velocity is a common indicator to validate Rayleigh–Taylor models. Second, the global convergence of the solution using a L^2 norm is studied for a series of uniformly refined meshes and also at a given moment in time.

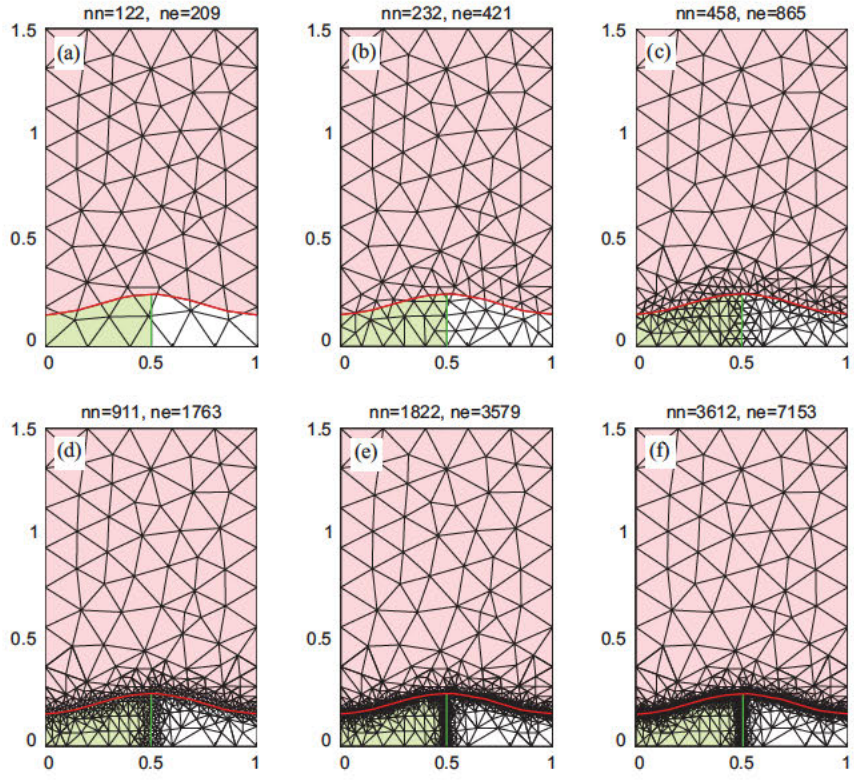

Fig. 10. Uniform mesh (a) and different levels of mesh refinement (b) to (f). All meshes correspond to the same moment during the evolution of different simulations. Number of nodes (nn) and number of elements (ne) are indicated for each mesh

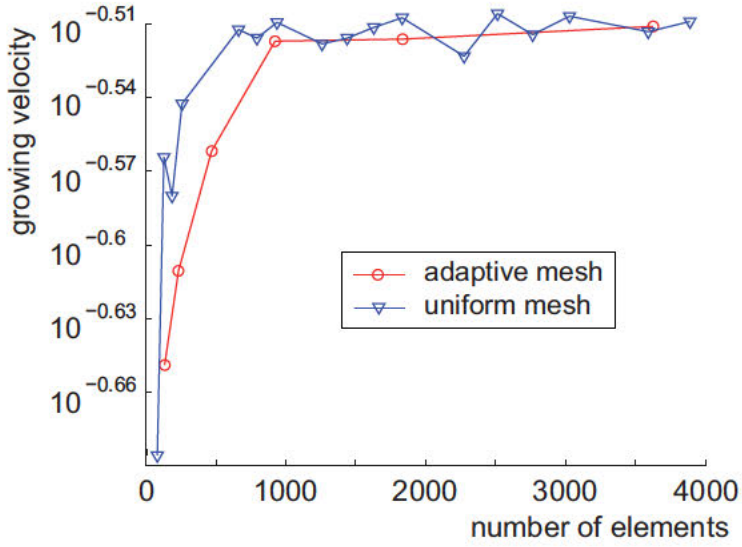

Fig. 11. Dependence of the velocity of the growing diapir with the mesh. Two series of meshes are shown: the triangles correspond to uniformly refined meshes, the circles correspond to adaptively refined meshes.

Some simple configurations of two–phase Rayleigh–Taylor instabilities allow for an analytical calculation of the growing velocity. This macroscopic velocity is a meaningful quantity of interest that can be compared with analogical experiments in some cases. Nevertheless, for the three-phase case no analytical solution is available. Therefore, no direct quantitative error assessment can be performed. A numerical convergence analysis is carried out for this problem. Figure 11 shows the convergence of the diapir growing velocity as a function of the number of elements in the mesh. The diapir growing velocity is calculated as the vertical ascending velocity of the triple junction point at a given moment in time which is a quantity of interest for the problem under consideration. This velocity generally coincides with the maximum velocity in all the domain. Two series of simulation are performed: one refining the mesh uniformly (marked with triangles), the other refining the mesh with an adaptive scheme near the interface (marked with circles). The mesh is adapted heuristically, using the multiphase character of the elements as remeshing indicator. In practice the elements crossed by one or more interfaces are subdivided performing a given number of recursive refinements. In the examples, see figure 10, five levels or recursivity are used. The adaptivity helps to converge faster and with less elements than the uniform refinement. A uniform mesh and several adaptive meshes with different refinement levels are displayed in Figure 10. The curve corresponding to the uniform refinement in figure 11 exhibits some oscillations. This is due to the fact that the quantity under consideration (growing velocity) is measured at a given time. The time step is set as a function of the Courant number and hence varies from mesh to mesh. Consequently, the exact time in which this velocity is computed slightly varies for the different points of the curve. However, the global behavior of the

curve seems to converge to the same value as the adaptive refinement and the oscillations are reduced as number of elements increases. The convergence is thus demonstrated for this standard quantity of interest in the diapir growing problem.

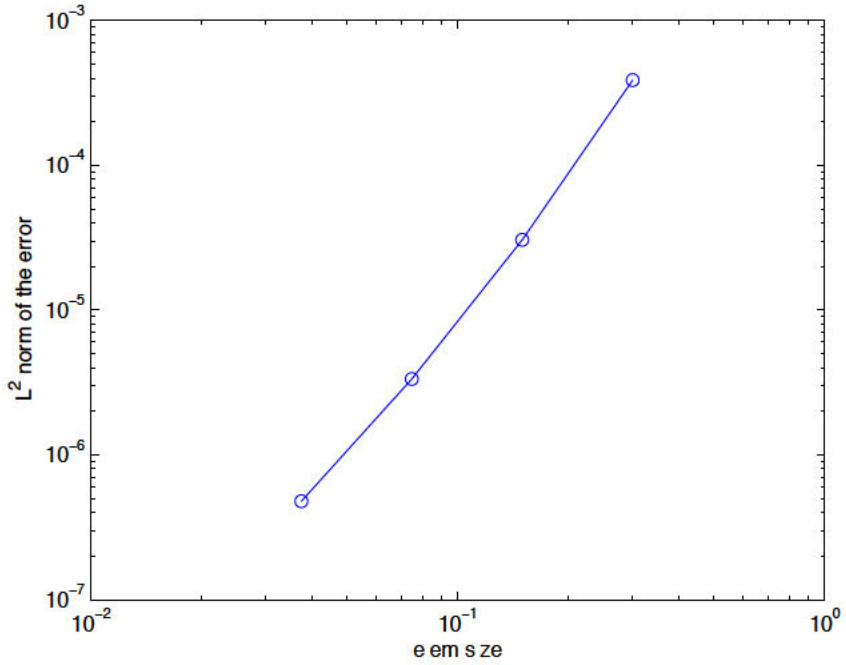

Fig. 12. L^2 error convergence of a steady state Stokes problem corresponding to one time step of the three-phase Rayleigh-Taylor instability (uniformly refined meshes).

The L^2 norm convergence is analyzed for the steady Stokes problem corresponding to the first time step of the three-phase instability problem. The analysis is carried out using five uniformly refined meshes. The finer one is used as a reference to assess the error of the remaining four. The resulting convergence plot is displayed in Figure 12. The obtained convergence rate follows the linear behavior observed in [5] using mini-element meshes ($P1^+$-P1) in two–phase problems. The approach presented here allows dealing with more than two phases while keeping the same convergence rate, without any loss of asymptotic accuracy.

An additional indicator of the consistency of the proposed scheme is the measure of the volume conservation. As a consequence of the incompressibility condition, each phase must conserve its initial volume and therefore all the observed discrepancies (loss or gain of volume) correspond to numerical errors. Thus, in order to assess the consistency of the scheme, the volume variation of each phase is tracked along the time evolution for a given mesh. For all the tested models, the observed volume variations are below 5%. And the larger deviations are only occurring after more than 100 time steps. These figures are

satisfactory, specially considering that no level set reinitialization procedure is used. Note however that the hierarchical level set approach would allow using any reinitialization procedure in a very simple manner because each level set function may be updated independently as for a standard two–phase model.

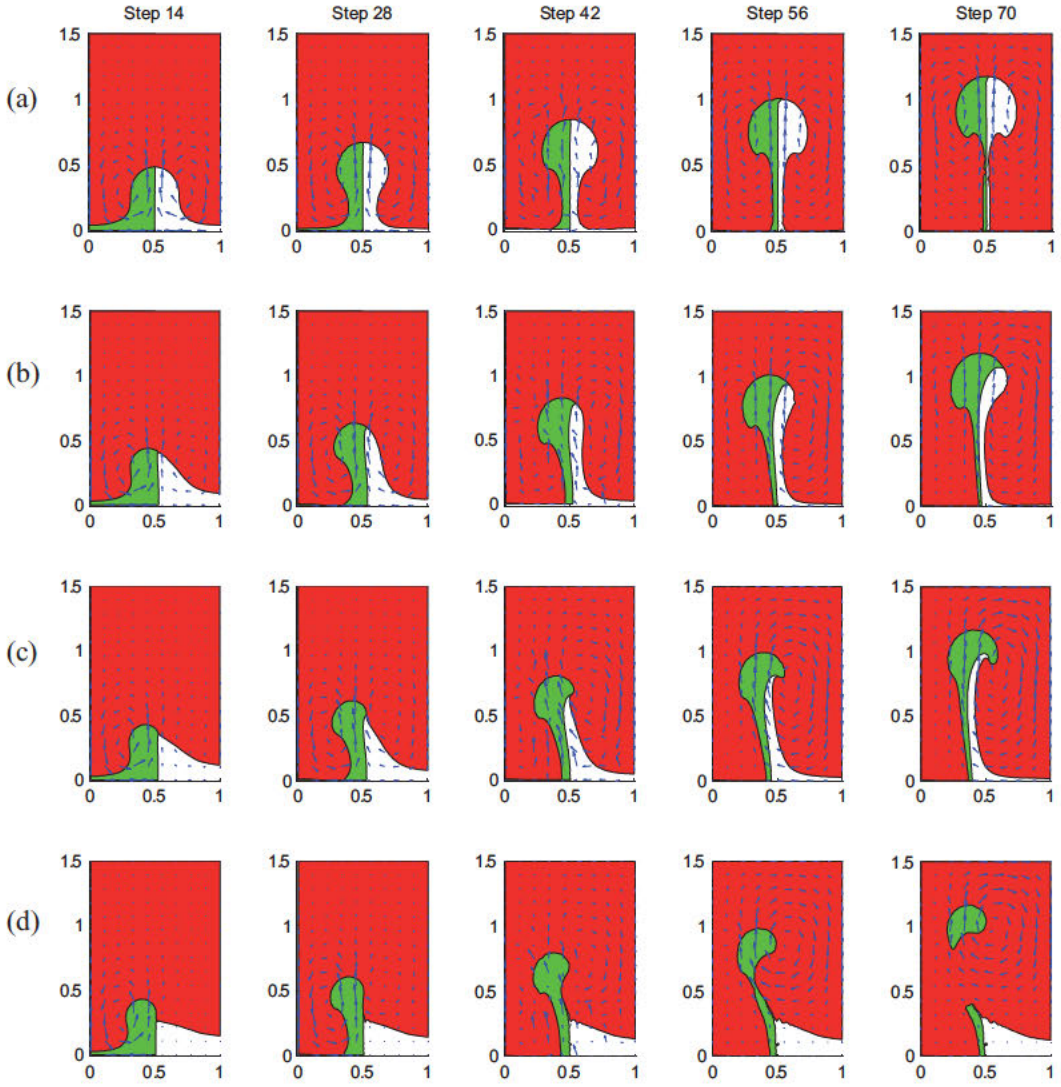

Fig. 13. Evolution of the 3–phase diapir. The models (a), (b), (c) and (d) differ in the viscosity of the lower right material, which is 1, 5, 10 and 100, respectively. The other two materials have viscosity $\eta = 1$. The upper denser layer has a density of 10, while the two buoyant lower materials have a density of 1.

The evolution of four models with different viscosity contrast between the two lower layers is shown in Figure 13. The (a) row corresponds to a model where all the materials have the same viscosity $\eta = 1$. In this conditions the two buoyant materials behave as a unique fluid and a standard symmetric diapir develops. The (b) row shows the evolution of the diapir when the viscosity of the right lower material is five times the viscosity of the left material. In this case the symmetry is lost. The evolution of the left half of the model is

similar to the (a) row while the right half of the model is controlled by the viscosity contrast between the right material and the overburden layer. The models of the third and fourth rows have a viscosity ratio between the two lower layers of 10 and 100, respectively. The very viscous right material of the last model is almost stopped, while the left material develops the diapir alone. In this example the main pattern of generated flow changes. In the early stages (1st and 2nd snapshots) the high viscosity of the right material inhibits the movement in the right half and the flow is concentrated in the left part of the domain. This bends the diapir to the left. Once the material gains enough height to loose the influence of the viscous layer (last two snapshots), the main flow moves to the right half of the model because there is more space facilitating the return flow. This latter inflexion bends the diapir rightward.

The conclusion on this qualitative test, is that the results show a complex behavior corresponding with the nature of the problem analyzed.

5.2 Three-dimensional instabilities

Two examples of gravitational instabilities in 3D are presented next. Firstly, a Rayleigh–Taylor instability similar to the 2D example of the previous section is presented. Secondly, an instability where the material phases lays horizontally is shown. In both cases the domain is a square box.

The first example involves three materials: an upper and denser phase, and two lower and buoyant fluids with a viscosity ratio of five between them. Same as in the previous case the level set $\phi^{(1)}$ (with highest hierarchy) determines the location of the upper material and has an initial sinusoidal perturbation to induce the development of the instability. The second level set represents the interface between the two lower fluids and is initially set parallel to one wall of the domain. A uniform structured mesh of 512 ($8 \times 8 \times 8$) 27-noded hexahedra is used in the simulations.

Figure 14 shows the location of both level sets after some time-steps. In panel (a) the two level sets are shown. Due to the hierarchy, the vertical level set is only relevant below the red surface. Panel (b) shows the same surfaces at the same time with the interface described by $\phi^{(1)}$ drawn in two different colors to emphasize the two lower materials and facilitate the comparison with the 2D model. Note that the contact between colors is where the second interface (described by $\phi^{(2)}$) intersects. This 3D example is comparable to the (b) row of Figure 13. A snapshot of the 2D model is included in panel (c), showing the comparable asymmetric pattern developed.

The second example, involves five different materials with the physical properties described in table 2. Contacts between these materials are described by

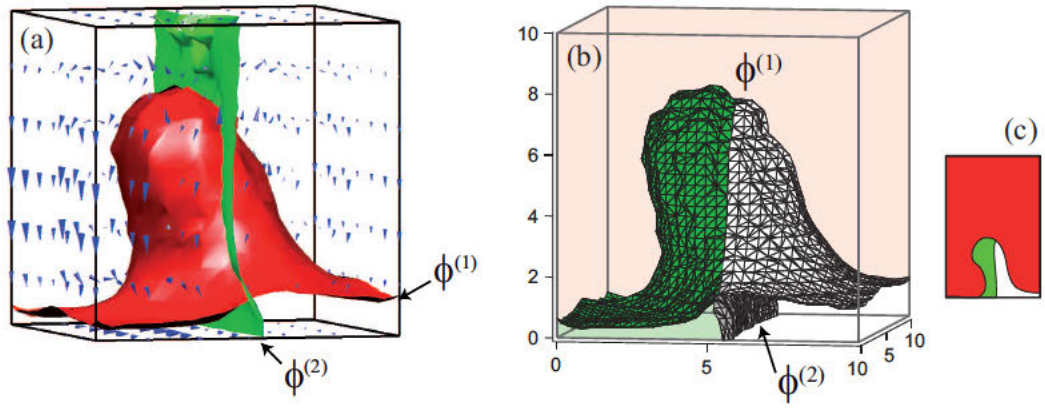

Fig. 14. Interfaces described by two level sets (a). The blue arrows show the velocity field. Colors in the upper surface of (b) show the contact between different materials. The generated shape coresponds to the 2D case shown in panel (c) (taken from figure 13 row (b)).

four level sets. The initial setup and two snapshots of the evolution are show in Figure 15 panels (a), (b) and (c).

Layer	Viscosity	Density
1	1	1
2	10	100
3	10	50
4	10	25
5	10	12

Table 2
Physical properties of materials for the layered 3D model. Layers are numbered bottom up.

Same as in the previous example, the lower phase is less dense than the overlying materials and a gravitational instability develops. In this case the buoyant lower material induces deformation in all the upper layers. Vertical cross-sections in the center of the model show how this deformation evolves (see Figure 15). A uniform non-structured mesh of 23461 four-noded tetrahedra elements is used in the simulations. The number of elements corresponds with a uniform mesh with 15 elements per side.

The two examples presented in this section show how the multiphase flow evolution is resolved when i) the level sets intersects each other and triple junction occurs inside one element, and ii) the level sets are parallel inside an element and are convected keeping parallelism. Both cases behave as consistently.

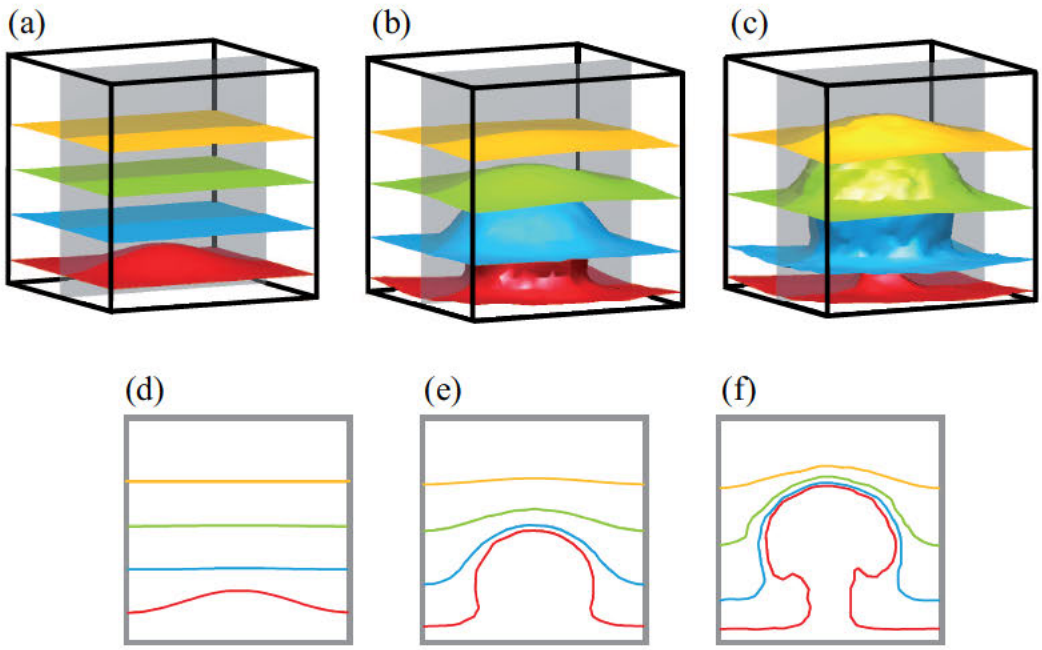

Fig. 15. Initial state (a) and snapshots (b) and (c) of the level set location during the evolution of the layered model. Panels (d), (e) and (f) show vertical cross-sections of the model, where the deformation of the layers is appreciated.

6 Concluding remarks

In this work the classical X–FEM is extended to handle n different materials. This approach is proposed here in the context of a n-phase flow problem but can be extended to other problems where the phases are described using level set and X–FEM. The location of the materials is described by an ordered collection of level set functions, for which a hierarchy is established. The enrichment of the solution is also restated to include cases where more than a single interface lies inside one element. To do this, a ridge function accounting for all level sets and the hierarchy between them is proposed.

A numerical study on the strategies to compute integrals in the multiphase elements is also carried out. An adaptive quadrature accounting for the interface location yields an approximation with sufficient accuracy.

The n-phase X–FEM approach is successfully applied to a multiphase flow problem in 2 and 3 dimensions, using triangular, tetrahedral and hexahedral elements.

Acknowledgements

This research has been supported by Ministerio de Educación y Ciencia, Grants DPI2007-62395, SAGAS CTM2005-08071-C03-03/MAR and the Spanish Team Consolider-Ingenio 2010 nrCSD2006-00041.

References

[1] J. Chessa and T. Belytschko. An extended finite element method for two–phase fluids. *Transactions of the ASME*, pages 10–17, 2003.

[2] C. Daux, N. Moes, J. Dolbow, N. Sukumar, and T. Belytschko. Arbitrary branched and intersecting cracks with the extended finite element method. *International Journal for Numerical Methods in Engineering*, 48:1741–1760, 2000.

[3] J. Donea and A. Huerta. *Finite Element Methods for Flow Problems*. Wiley, Chichester, West Sussex PO19 8SQ, England, 2002.

[4] A. Gerstenberger and W. A. Wall. An extended finite element method /lagrange multiplier based approach for fluid-structure interaction. *Computer Methods in Applied Mechanics and Engineering*, in press:(doi:10.1016/j.cma.2007.07.002), 2007.

[5] G. Legrain, N. Moës, and A. Huerta. Stability of incompressible formulations enriches with X–FEM. *Computer Methods in Applied Mechanics and Engineering*, 197:1835–1849, 2008.

[6] N. Moës, M. Cloirec, P. Cartaud, and J. F. Remacle. A computational approach to handle complex microstructure geometries. *Computer Methods in Applied Mechanics and Engineering*, 192:3163–3177, 2003.

[7] S. Osher and R. Fedkiw. Level set methods: an overview and some recent results. *Journal of Computational Physics*, 169:463–502, 2001.

[8] S. Osher and J.A. Sethian. Front propagating with curvature dependent speed: algorithms based on hamiltonjacobi formulations. *Journal of Computational Physics*, 79:12–49, 1988.

[9] S. J. Ruuth. A diffusion–generated approach to multiphase motion. *Journal of Computational Physics*, 145:166–192, 1998.

[10] J.A. Sethian and P. Smereka. Level set methods for fluid interfaces. *Annual Review of Fluid Mechanics*, 35:341–372, 2003.

[11] L. Tan and N. Zabaras. A level set simulation of dendritic solidification of multi-component alloys. *Journal of Computational Physics*, 221:9–40, 2007.

[12] G. J. Wagner, N. Moës, W. K. Liu, and T. Belytschko. The extended finite element method for rigid particles in Stokes flow. *International Journal for Numerical Methods in Engineering*, 51(3):293–313, 2001.

[13] H.-K. Zhao, T. Chan, B. Merriman, and Osher. A variational level set approach to multiphase motion. *Journal of Computational Physics*, 127:179–195, 1996.

[14] S. Zlotnik, P. Díez, M. Fernández, and J. Vergés. Numerical modelling of tectonic plates subduction using X–FEM. *Computer Methods in Applied Mechanics and Engineering*, 196:4283–4293, 2007.